IOP Publishing Journal of Physics D: Applied Physics
J. Phys. D: Appl. Phys. **54** (2021) 505302 (10pp) https://doi.org/10.1088/1361-6463/ac1ec3

Thermal transport of amorphous phase change memory materials using population-coherence theory: a first-principles study

Lei Yang and Bing-Yang Cao*

Key Laboratory of Thermal Science and Power Engineering of Ministry of Education, Department of Engineering Mechanics, Tsinghua University, Beijing 100084, People's Republic of China

E-mail: caoby@tsinghua.edu.cn

Received 20 June 2021, revised 3 August 2021
Accepted for publication 18 August 2021
Published 17 September 2021

Abstract

Thermal conduction plays a vital role in applications of phase change memory (PCM) materials. Phonon-based theory and the Wiedemann–Franz–Lorenz rule have been widely utilized to describe the thermal transport in crystalline PCM materials, while the understanding of heat conduction in the amorphous phase remains insufficient. Here, we quantify the contributions of the coherences (coupling of vibrational modes) and populations (phonon-like) to the thermal conduction of amorphous $Ge_2Sb_2Te_5$ (GST) and $GeTe_4$, two kinds of typical PCM materials. The contributions of the coherences and populations are calculated using the theory proposed by Allen and Feldman (AF theory) and the single-mode relaxation time approximation of the Boltzmann transport equation based on first-principles calculations. Our results demonstrate that coherences contribute more than 97% of the total thermal conductivities for both amorphous GST and $GeTe_4$ above Debye temperature, while the populations' contribution is negligible. Besides, the temperature dependence of the thermal conductivities is predicted and analyzed, allowed by the AF theory with the mode linewidths-dependent broadening method introduced in this paper. The predicted positive temperature dependence of amorphous $GeTe_4$ above Debye temperature, in good agreement with the experimental results, is due to the unique nature of coherences, i.e. larger contribution to heat conduction from stronger couplings between different normal modes at a higher temperature. Our calculation provides new insight into thermal transport in amorphous PCM materials and reveals the physical mechanisms of temperature-dependent thermal conductivities above Debye temperature, and the calculation framework can also be extended to other disordered systems.

Keywords: thermal transport, thermal conductivity, population and coherence, phase change memory materials

(Some figures may appear in color only in the online journal)

* Author to whom any correspondence should be addressed.

1. Introduction

Chalcogenide phase change memory (PCM) materials have been widely investigated for applications in rewriteable optical storage and electronic nonvolatile memory for decades because of their unique fast and reversible phase change characteristics between crystalline and amorphous states with significantly different optical or electrical properties [1–4]. The phase changes are implemented by fast heating and cooling processes induced by applying an appropriate electrical current or laser pulse [2, 5]. For PCM technology, the thermal transport properties of PCM materials will determine the switching time, cyclability, retention period, power consumption, and reliability of memory devices [6–10]. Therefore, it is crucial to quantitatively characterize the thermal conductivity of PCM materials, that is closely related to the heat transport phenomenon, and to dissect the influencing factors as well as underlying thermal transport mechanisms.

The thermal conductivities of typical PCM materials, including $Ge_2Sb_2Te_5$ (GST), GeTe, and $GeTe_4$, were measured with optical [11–17] and electrical [18–25] methods. A considerable number of results have been reported. Due to the different fabrication conditions, sample thicknesses, and measurement techniques, the reported thermal conductivity data of both crystalline and amorphous phases vary in a wide range. Thus, theoretical and computational studies on the thermal conductivity of PCM materials are necessary to reveal the underlying thermal transport mechanisms. For the crystalline PCM materials, the Wiedemann–Franz–Lorenz rule has been widely used to describe the electron contribution to thermal conductivity [6, 26], and the phonon Boltzmann transport equation (PBTE) with well-developed solution methods in recent years on its linearized form [27–29] has allowed reliable prediction on the lattice thermal conductivity based on first-principles calculations [17, 30–32]. As for the amorphous PCM materials, the electron contribution to the thermal conductivity can be neglected because the electrical conductivity of the amorphous phase is orders of magnitude lower than that of the crystalline phase, while the vibrational thermal conductivity is inadequately studied or understood due to the lack of long-range order and the elusive physical picture for heat conduction in amorphous materials. An available calculation method is approach-to-equilibrium molecular dynamics (AEMD). The time evolution of temperature difference in the studied system is monitored after a nonequilibrium initialization to predict thermal conductivity [27]. First-principles AEMD simulations have been employed to predict the thermal conductivities of amorphous GST [9, 33] and $GeTe_4$ [34–36] and to analyze the size effect combined with an empirical model [33, 36]. A significant temperature difference is indispensable for the AEMD method, so the temperature dependence of thermal conductivity was totally ignored. The maximum temperature during the simulation even exceeded the crystallization temperature [9], which might cause the structural transition inevitably. Hence, more reliable simulation methods capable of considering the temperature dependence of thermal conductivity are still needed for amorphous PCM materials. Besides, further analyses are necessary to promote the understanding of the thermal transport in amorphous PCM materials, based on more fundamental theoretical modeling and a compelling physical picture.

One physical picture of thermal conduction in amorphous materials is random walks of energy between neighboring atoms vibrating, as proposed by Einstein [37]. Based on the random walking picture, Slack proposed the minimum thermal conductivity (MTC) model [38], and Cahill *et al* further derived a widely-used formula [39] based on the Debye model of lattice vibration. Although the MTC model prediction agrees well with the experimental data of many amorphous materials [40–43], including amorphous PCM materials [10, 11, 17], at room temperature, the predicted temperature dependence of thermal conductivity far above Debye temperature is almost constant and not consistent with the significantly positive variation tendency from experimental measurements in some amorphous materials [44, 45], such as amorphous $GeTe_4$ [25]. The positive temperature dependence indicates that different thermal transport mechanisms might exist. The theory proposed by Allen and Feldman (AF theory) reveals the new thermal conduction mechanism, i.e. coupling between different vibrational modes [46], by considering the nondiagonal part of the heat-flux operator [47]. The derived formula of thermal conductivity in AF theory consists of an intra-band part and an inter-band part. The intra-band part describes the phonon-like contribution to thermal conduction, while the inter-band part corresponds to the new thermal conduction mechanism. Simoncelli *et al* also derived a general transport equation from the Wigner phase space formulation of quantum mechanics [48] to describe this new conduction mechanism. Populations and coherences, corresponding to the intra-band and inter-band part in AF theory, were proposed and used to classify the thermal conduction [48]. The populations' contribution can be calculated by the single-mode relaxation time approximation (SMA) of PBTE in the kinetic regime, and the coherences' part could reduce to the AF theory in the harmonic limit [48]. AF theory has been widely employed to predict the coherences' contribution to thermal conductivity, called diffusons' contribution in [49,50], for amorphous [10, 51–53] and complex crystalline [54] materials. However, the difference in coupling strength at different temperature and frequency ranges were neglected due to the Lorentzian broadening with a constant half-peak width for practicality. Due to the lack of consideration of anharmonic effects, the temperature dependence of thermal conductivity deviated from the experimental results in the high-temperature range [25, 45]. Thus, a temperature and frequency-dependent broadening method may be necessary for AF theory [51] and potential to overcome the harmonic limit, especially when the temperature dependence is significant.

In this paper, we adopt the SMA method and AF theory to quantify the populations' and coherences' contributions to the thermal conduction of amorphous GST and $GeTe_4$. Sosso *et al* have used a similar framework to calculate the thermal conductivity of amorphous GeTe based on molecular dynamics (MD) simulations [10] with a machine-learning-based interatomic potential [55]. They found that the size effect of amorphous GeTe could be ignored, and this conclusion is also

conceivable for other Ge–Sb–Te compounds. Due to the lack of reliable interatomic potentials for GST and $GeTe_4$, first-principles calculations are carried out to generate the amorphous structures and to obtain the interatomic force constants. The other important motivation of this paper is to analyze the temperature-dependent thermal conductivities of amorphous PCM materials, especially above the Debye temperature. A mode linewidths-dependent broadening method is introduced for AF theory in this paper and applied in the amorphous $GeTe_4$ case. The rest of this paper is structured as follows. The theoretical formulations and calculation details are presented in section 2. The results, including structure characterization and validation, mode-level properties, and thermal conductivities of amorphous GST and $GeTe_4$, are given and discussed in section 3. Finally, the conclusions are summarized in section 4.

2. Theoretical formulation and calculation details

Unlike the case in which phonons dominate the heat conduction in crystalline semiconductors or insulator materials, the coherences' contribution from the coupling of vibrational modes is always non-ignorable for amorphous materials due to the disorder structures and ultralow phonon-like contribution [56, 57]. AF theory has been employed in the frameworks based on MD simulations [10, 49,51–53] or first-principles calculations [54]. By considering the nondiagonal part of the heat-flux operator [47], Allen and Feldman presented the Kubo formula of thermal conductivity [46, 58] and split it into an intra-band part and an inter-band part, corresponding to the contributions from populations and coherences in [48]. The populations' contribution reduces to the SMA result in the kinetic regime, i.e.

$$\kappa_{\mathrm{P}} = \kappa^{\mathrm{SMA}} = \frac{1}{3V}\sum_i C(\omega_i)\, v_{gi}^2 \tau_i. \tag{1}$$

Equation (1) is widely used in crystals and can also describe the phonon-like contribution in amorphous materials in many cases. In equation (1), C is mode specific heat determined by

$$C(\omega) = -\frac{\partial \bar{n}}{\partial \omega}\frac{\hbar\omega^2}{T} = k_{\mathrm{B}}\left[\frac{\hbar\omega/2k_{\mathrm{B}}T}{\sinh\left(\hbar\omega/2k_{\mathrm{B}}T\right)}\right]^2, \tag{2}$$

v_{g} is group velocity from the lattice dynamics calculation, and the lifetime τ is calculated by

$$\tau_i = \frac{1}{2\Gamma_i^{\mathrm{NMD}}}. \tag{3}$$

Γ_i^{NMD} is the mode linewidth from normal mode decomposition (NMD), which can be predicted by fitting spectral energy density to a Lorentzian function

$$E_i(\omega) = A_i\frac{\Gamma_i^{\mathrm{NMD}}}{\left[\omega_i-\omega\right]^2+\Gamma_i^{\mathrm{NMD}}} \tag{4}$$

where E_i is mode spectral energy calculated by mapping atomic trajectories from an MD simulation onto vibrational mode coordinate time derivatives, and more details can be found in [51, 59].

The coherences' contribution was derived as a widely used compact formula [46]

$$\kappa_{\mathrm{C}} = \kappa^{\mathrm{AF}} = \frac{1}{V}\sum_i C_i D_i^{\mathrm{AF}} \tag{5}$$

by introducing the mode diffusivity

$$D_i^{\mathrm{AF}} = \frac{\pi V^2}{3\hbar^2\omega_i^2}\sum_{j\neq i}\left|\boldsymbol{S}_{ij}\right|^2\delta\left(\omega_i-\omega_j\right). \tag{6}$$

The mode diffusivities describe the contribution to the heat conduction from coherences, i.e. coupling between vibrational modes, different from phonon-like propagation. For amorphous materials, in the case of gamma point and with only one large cell considered, the heat-flux operator is formulated as

$$\boldsymbol{S}_{ij} = \frac{\hbar}{2V}\boldsymbol{v}_{ij}\left(\omega_i+\omega_j\right) \tag{7}$$

and

$$\boldsymbol{v}_{ij} = \frac{1\cdot i}{2\sqrt{\omega_i\omega_j}}\sum_{\alpha,\alpha'}\sum_{k,k'} e_{i,k\alpha}D_{k'\alpha',k\alpha}\times\boldsymbol{R}_{kk'}\times e_{j,k'\alpha'} \tag{8}$$

where $D_{k'\alpha',k\alpha}$ is the dynamic matrix element, $e_{i,k\alpha}$ is the eigenvector element, $\boldsymbol{R}_{kk'}$ is the distance between different atoms. Substituting equations (6)–(8) into equation (5) leads to

$$\kappa_{\alpha\beta}^{\mathrm{AF}} = \frac{1}{V}\frac{\pi\hbar^2}{k_BT^2}\sum_i\left[\overline{n}_i\left(\overline{n}_i+1\right)\sum_{j,j\neq i}\frac{\left(\omega_i+\omega_j\right)^2}{4}v_{ij}^{\alpha}v_{ij}^{\beta}\delta\left(\omega_i-\omega_j\right)\right], \tag{9}$$

which has been proved equal to the exact expression of the coherences' contribution from the Wigner phase space formulation of quantum mechanics in harmonic limit [48]. The coherences' contribution is expressed as [48]

$$\kappa_{\alpha\beta}^{\mathrm{C}} = \frac{1}{V}\sum_{i,j(i\neq j)}\left\{\frac{\hbar^2\pi}{k_{\mathrm{B}}T^2}\frac{\omega_i+\omega_j}{2}\left[\omega_i\overline{f}_i\left(\overline{f}_i+1\right)+\omega_j\overline{f}_j\left(\overline{f}_j+1\right)\right]V_{ij}^{\alpha}V_{ji}^{\beta}\times\frac{\frac{\Gamma_i+\Gamma_j}{2}/\pi}{\left(\omega_i-\omega_j\right)^2+\left(\frac{\Gamma_i+\Gamma_j}{2}\right)^2}\right\}. \tag{10}$$

The velocity operators in equations (9) and (10) are related by [48]

$$v_{ij}^{\alpha} = \frac{\omega_i+\omega_j}{2\sqrt{\omega_i\omega_j}}V_{ij}^{\alpha}. \tag{11}$$

AF theory considers couplings only between degenerate eigenstates due to the nature of the δ function in equation (9), and the difference in coupling strength at different temperature and frequency ranges are neglected. To overcome such a

problem, we broaden the δ function in equation (9) in a different way from the previous constant half-peak width inspired by the term

$$\delta_{\text{anh}} = \frac{\frac{\Gamma_i+\Gamma_j}{2}\Big/\pi}{(\omega_i-\omega_j)^2+\left(\frac{\Gamma_i+\Gamma_j}{2}\right)^2} \tag{12}$$

which embodied the anharmonic effect in equation (10). A Lorentzian formula

$$\delta_b(\omega_i-\omega_j) = \frac{\Gamma_{ij}^{\text{AF}}\Big/\pi}{(\omega_i-\omega_j)^2+\left(\Gamma_{ij}^{\text{AF}}\right)^2}, \tag{13}$$

is used, and the half-peak width Γ_{ij}^{AF} is related to NMD linewidths of involved modes by

$$\Gamma_{ij}^{\text{AF}} = \xi\frac{\left(\Gamma_i^{\text{NMD}}+\Gamma_j^{\text{NMD}}\right)}{2}. \tag{14}$$

Consequently, the temperature and frequency dependence of coupling between different vibrational modes can be considered in the AF theory framework by using linewidths predicted for all the vibrational modes at the corresponding temperature from NMD. We attribute the existence of a constant ξ in equation (14) to the finite size of simulation systems. It is worth noting that such an NMD linewidths-dependent broadening method enables AF theory to consider the temperature dependence of thermal conductivity resulting from the varying coupling of vibrational modes with temperatures, i.e. the anharmonic effect.

Based on the above derivations and analyses, we calculate the thermal conductivity of amorphous PCM materials by

$$\kappa_{\text{V}} = \kappa_{\text{P}} + \kappa_{\text{C}}, \tag{15}$$

and quantify the populations' (κ_{P}) and coherences' contributions (κ_{C}) by equations (1) and (9), respectively. The samples of amorphous GST and $GeTe_4$ are generated by a melt-quench process based on *ab initio* molecular dynamics (AIMD) simulations. Specifically, initial samples are melted at 3000 K first to randomize the structures, then quenched to 300 K, similar to the real quenching process, and finally equilibrated for 10 ps at 300 K in the canonical ensemble (NVT). After the amorphous structures are generated and then relaxed as much as possible, the finite difference method is used to calculate the interatomic force constants. The lattice dynamics and NMD calculations are then carried out to get mode-level properties, and the required atomic trajectories for linewidths and lifetimes prediction are from 100 ps AIMD simulations in the microcanonical ensemble (NVE) at various temperatures. All the first-principles calculations, including AIMD simulations, structure relaxation, and force constants calculations [60, 61], are performed with a Vienna *ab initio* Simulation Package (VASP) [62] using projective augmented wave (PAW) pseudopotential [63] and the generalized gradient approximation in the Perdew–Burke–Ernzerhof (PBE) [64] form for the exchange-correlation functional. Phonopy [65] is also used for lattice dynamics calculation.

3. Results and discussion

3.1. Structure characterization and validation

For amorphous materials, radial distribution functions (RDFs) are widely used to characterize the short-order range, and structure factors calculated by inverse Fourier transform of RDFs are usually compared with the neutron or x-ray diffraction patterns to check the reliability of the simulated structure [66]. Amorphous GST samples, including 225-atom samples generated from the AIMD melt-quench procedure in this paper and 315-atom samples generated using Gaussian approximation potential (GAP) in [67], are relaxed with and without van der Waals (vdW) interactions correction, [68] respectively, for further structure characterization. The neutron structure factors of the four samples mentioned above are calculated and compared with the experimental results [69] in figure 1(a). The four cases do not show significant differences, and all agree well with the experimental results, except the first sharp diffraction peak (FSDP) at around 1.1 Å^{-1}, which is related to the medium-range order in such a system [67]. A larger model might be necessary, but the larger model with 7000 atoms generated by GAP-based MD only showed a modest FSDP [67]. Such a large model is also beyond the capacity of first-principles calculations, so we do not excessively expect the same structure factor patterns from first-principles calculations as from the experimental results.

The RDFs of these four models are also calculated to analyze the local structure of amorphous GST further. As shown in figure 1(b), the RDFs of the models generated by AIMD and GAP-based MD show no difference either with or without vdW correction, while the cases with vdW correction possess a clearly smaller position of the second RDF peak. Considering that RDF peak positions are closely related to distances between neighboring atoms, the density evolutions of the cases with and without vdW correction are checked during AIMD simulations in the isothermal–isobaric (NPT) ensemble, as shown in figure 1(c). The same initial models with a density close to the value reported in the previous experiments (5.87 g cm^{-3} [70]) are adopted. It turns out that the density in the case without the vdW correction decreases to a significantly lower value while the density in the case with vdW correction retains close to the value from the experiments. vdW interactions correction has been proved necessary and influences the dispersion relationship calculation for the first-principles calculations on crystalline GST in the GGA schemes [30, 32] due to lack of consideration on vdW interactions. The comparisons here further demonstrate that vdW interactions also matter in amorphous GST, and it is essential to consider vdW interactions correction for first principles-calculation in the GGA schemes.

An amorphous $GeTe_4$ sample with 250 atoms is also generated by the AIMD-based melt-quench process and then relaxed with vdW correction. As shown in figure 1(d), the structure factor of the amorphous $GeTe_4$ sample agrees well with the experimental results [71], apart from the position of the first diffraction peak, which might be due to the sensitivity to the choice of exchange-correlation functional and vdW

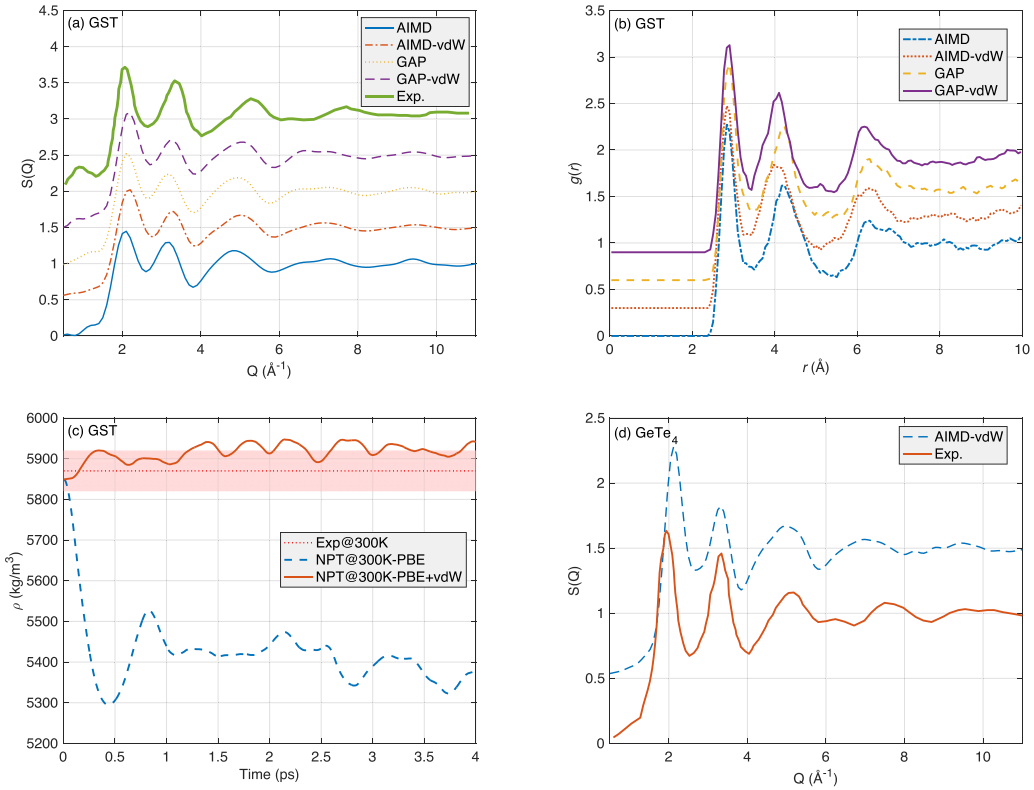

Figure 1. (a) Neutron structure factors of amorphous GST from experiments [69] and calculated for different samples, shifted up to be clear (AIMD: 225-atom sample generated from AIMD based melt-quench process and relaxed without vdW correction; AIMD-vdW: 225-atom sample generated from AIMD based melt-quench process and relaxed with vdW correction; GAP: 315-atom sample generated based on GAP from [67] and relaxed without vdW correction; GAP-vdW: 315-atom sample generated based on GAP and relaxed with vdW correction). (b) Radial distribution functions for different amorphous GST samples. (c) Density evolution of the simulated 225-atom GST model generated from AIMD based melt-quench process in an isothermal–isobaric (NPT) ensemble at 300 K, with vdW correction (NPT@300 K-PBE + vdW) versus without (NPT@300 K-PBE), compared with the measured density in [70] (Exp.@300 K). (d) Neutron structure factors of amorphous $GeTe_4$ from experiments [71] (Exp.) and calculated for the 250-atom sample generated from melt-quench process based on AIMD simulations and relaxed with vdW correction (AIMD-vdW), shifted up to be clear.

correction method. The analyses on different approaches in [72] demonstrate that schemes accounting for vdW interactions are not univocal, and the impact of vdW correction is still debatable. Therefore, we do not search for a perfect comparison with the measured structure factors.

3.2. *Vibrational mode properties*

Mode-level properties of all vibrational modes are calculated for each sample based on lattice dynamics and NMD calculations to quantify the populations' and coherences' contributions. Group velocities, lifetimes, linewidths, and diffusivities of an amorphous GST sample (with 225 atoms, generated from an AIMD melt-quench process and relaxed with vdW interactions correction) are shown in figures 2(a)–(d) to illustrate the underlying details and to conduct further analyses. For the prediction of the populations' contribution based on equation (1), group velocities and lifetimes are required. Effective group velocities at the gamma point are averaged from group velocities of the points near the gamma point in a uniform grid, similar to [10]. As shown in figure 2(a), the frequency-dependent group velocities converge to a value close to the sound speed of amorphous GST, 2250 m s^{-1} [11], in a low-frequency limit, while the group velocities of the most vibrational modes are orders of magnitude smaller than those in crystalline GST [30], and much smaller than the sound speed assumed in MTC model [39]. The exceptionally low group velocities of amorphous GST can limit the phonon-like populations' contribution to thermal conduction. In NMD calculations, the mode lifetimes are related with mode linewidths by equation (3), and the linewidths are fitted from the spectral energy distribution functions of vibrational modes, clearly Lorentzian-like in our calculations. The predicted lifetimes and linewidths at 300 K are presented in figures 2(b) and (c), respectively. The lifetimes of most vibrational modes are between one and three times the period of vibration ($2\pi/\omega - 3 \times 2\pi/\omega$), as illustrated in figure 2(b). The values of the mode lifetimes are several times larger than half the period of vibration assumed in the MTC model [39], significantly lower than those of ideal crystalline GST, but comparable with the lifetimes of crystalline GST with some point disorders, like vacancies and Ge/Sb atom translocation, reported in [30]. The analyses on the mode-level group velocities and lifetimes show that the populations' contribution in amorphous GST is different from that in the crystalline phase, mainly in group velocities, due to the lack of space periodicity. Compared with the MTC model, the mode

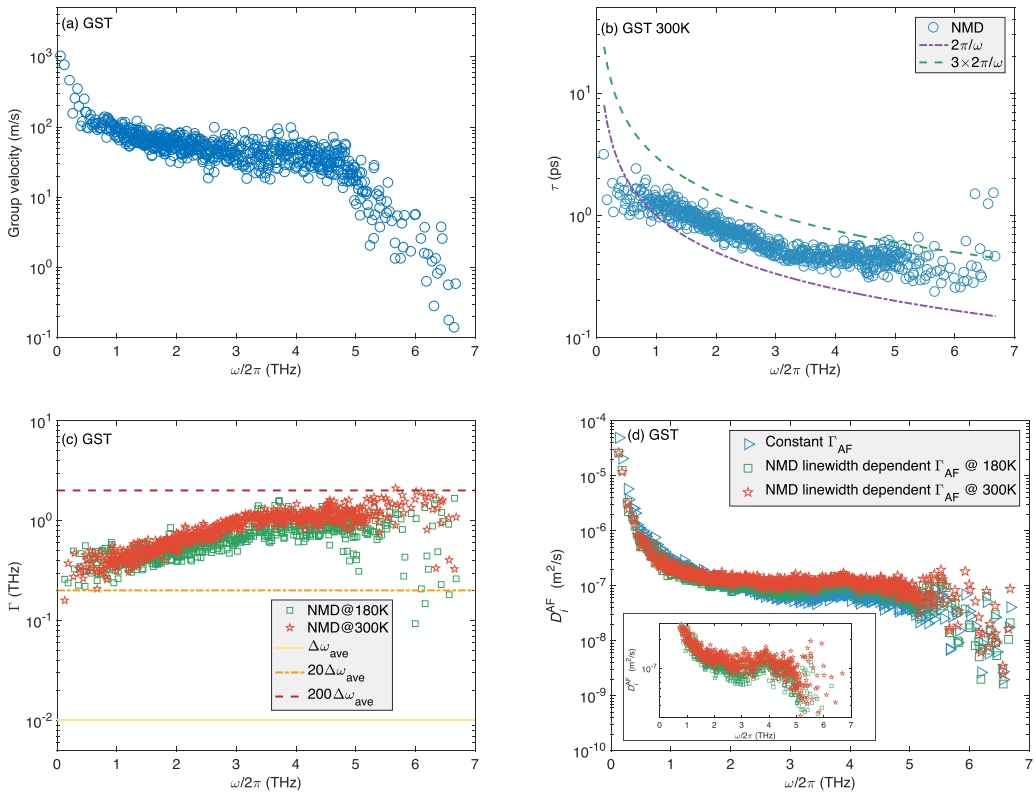

Figure 2. (a) Mode group velocities predicted from lattice dynamics for amorphous GST. (b) NMD-predicted mode lifetimes for amorphous GST at 300 K. (c) NMD-predicted mode linewidths for amorphous GST at 300 K. (d) Diffusivities based on AF theory for amorphous GST at 300 K with NMD linewidths-dependent broadening at 180 K and 300 K, versus with constant broadening.

group velocities are significantly lower while the lifetimes are of the same magnitude, so a lower phonon-like populations' contribution is expected in this paper.

Diffusivities are needed to predict the coherences' contribution by AF theory. For practical implementations of finite simulation systems, δ function in equation (9) must be broadened. The Lorentzian function with constant half-peak width ($\Gamma_{ij}^{\mathrm{AF}}$) equal to several times the mean level spacing of vibrational modes frequency ($\Delta\omega_{\mathrm{ave}}$) has been used for different disordered materials in previous research [10, 51–53], nonetheless, without a unified and reasonable determination method [48, 54]. In section 2, we have introduced the frequency and temperature-dependent broadening method, which relies on the mode linewidths predicted by NMD. As presented in figure 2(c), the predicted mode linewidths at 180 K and 300 K are in the range from 20 to 200 times of $\Delta\omega_{\mathrm{ave}}$ and exhibit positive frequency and temperature dependence. AF diffusivities at corresponding temperatures are calculated according to equations (6), (13) and (14) 13, shown in figure 2(d). The diffusivities based on the constant broadening method with a width of $5\Delta\omega_{\mathrm{ave}}$ recommended for amorphous silica and some other disordered systems [51, 53] are also given for comparison. ξ in equation (14) is determined to make the average broadening width equal to that of the constant broadening method. Compared with the constant broadening method, the NMD linewidths-dependent broadening predicts smaller diffusivities at low-frequency range while predicts larger diffusivities at the high-frequency range due to the different mode linewidths. The variation of diffusivities with temperature (see the inset of figure 2(d)) can also be predicted by AF theory with NMD linewidths dependent broadening and finally results in the temperature dependence of thermal conductivities. The new NMD linewidths-dependent broadening method allows us to consider the anharmonic effects of coherences in AF theory, described by the term δ_{anh} (see equation (12)) in the universal formula of coherences contribution in [48].

3.3. *Thermal conductivities of amorphous PCM materials*

The thermal conductivity of amorphous GST at 300 K is predicted from various cases and plotted in figure 3(a), including the populations' and coherences' contributions. Considering the quenching rate-dependent chemical order of amorphous PCM materials in the GAP-based MD simulations [73, 74], we predict the thermal conductivities of samples with 225 atoms generated at various rates, from 500 K ps^{-1} to 5 K ps^{-1}. No evident dependence of thermal conductivities on the quenching rate is found, and we also make a statistical inference based on the Pearson correlation coefficient with the null hypothesis that the correlation is zero [75]. It turns out that the p-value is 0.7338 and the null hypothesis should be accepted, which supports the conclusion that the predicted thermal conductivity is independent on the quenching rate. We attribute the quenching rate independence to the 10 ps NVT equilibrium at 300 K and structure relaxation before the calculation of interatomic force constants, which remove most of the metastability and

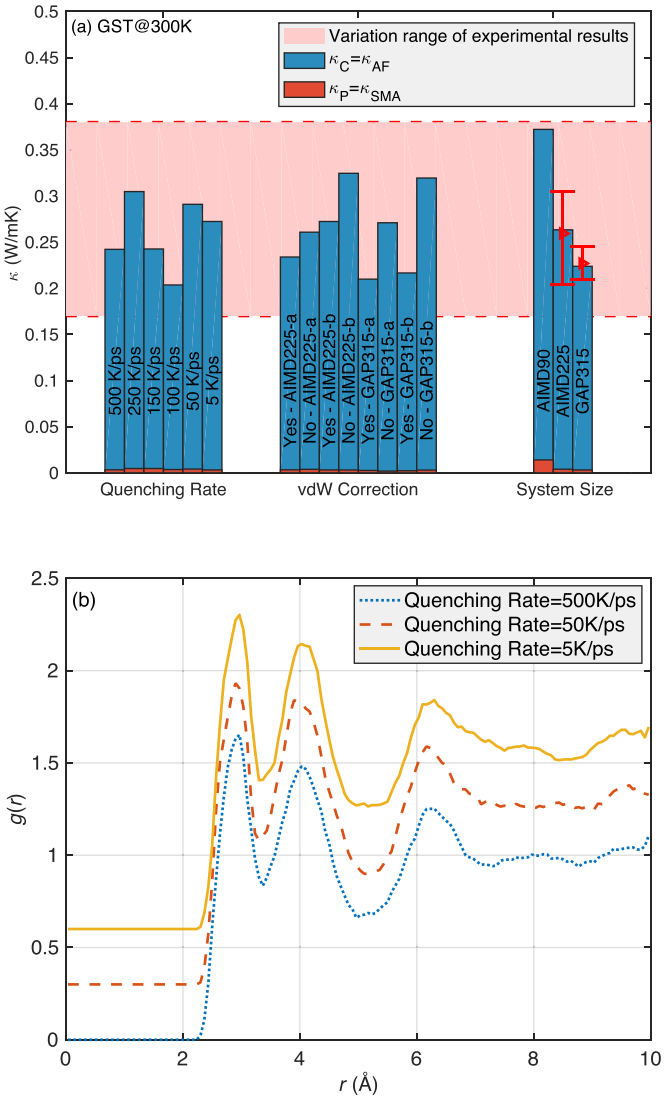

Figure 3. (a) Thermal conductivity prediction results of GST at 300 K in different cases: generated at various quenching rates; relaxed with and without vdW correction for samples generated based on AIMD or GAP; with various system size (with 90, 225 and 315 atoms). (b) Radial distribution functions for the amorphous GST samples generated at various quench rates (500 K ps^{-1}, 50 K ps^{-1} and 5 K ps^{-1}).

different chemical order in the cases at various quenching rates. This explanation is based on the comparison of the RDFs from samples quenched at various quenching rates. As shown in figure 3(b), no difference of RDF peaks exists in the cases at different quenching rates, unlike the situations of vdW correction showed in figure 1(b). The influence of vdW interaction correction on thermal conductivity is also reported in figure 3. The thermal conductivity in the case relaxed with vdW correction is lower than that without vdW correction for both AIMD and GAP-based samples. We use the point-biserial correlation coefficient to test the null hypothesis that the correlation between thermal conductivity and vdW correction is zero [76]. The p-value is 0.03, so the null hypothesis should be rejected at the 5% significant level, a widely-used criteria in statistics. The results here confirm the necessity of vdW correction for thermal conductivity calculation, besides the structure generation discussed in section 3.1. Hence, the final results reported here are from the cases with vdW correction. For all the cases, the populations' contributions are all lower than 0.005 W m^{-1} K^{-1}, which are negligible and agree with the conclusions from MD-based calculations on amorphous GeTe [10], apart from the 90-atom system. The larger populations' contribution (0.014 W m^{-1} K^{-1}, 3.9%) of the sample with 90 atoms possibly results from the relatively larger influence of periodic boundary conditions, and the quite different coherences' contribution possibly results from the limited modes quantity due to the finite size. For both 225-atom samples (generated based on AIMD) and 315-atom samples (generated based on GAP), the values reported in the system size group in figure 3 are averaged from independent structures, with the error bars estimated conservatively by the range statistics. The reported values for 225-atom samples and 315-atom samples are consistent with each other and in agreement with the experimental results. Thus, we conclude that both 225-atom samples and 315-atom samples are large enough to describe the disordered structure and proper to be used to predict the thermal conductivity of amorphous GST. We finally report that the thermal conductivity of amorphous GST at 300 K is 0.25 ± 0.04 W m^{-1} K^{-1}, in which the populations' contribution is 0.004 ± 0.001 W m^{-1} K^{-1} (∼1.5%) and the coherences' contribution is 0.244 ± 0.035 W m^{-1} K^{-1} (∼98.5%), based on the results of all 225-atom and 315-atom samples relaxed with vdW correction. The results mean that coherences' contribution to the thermal conductivity is dominant, and the characteristics of the thermal conduction, like temperature dependence, will be determined by coherences in amorphous GST.

Due to the lack of enough experimental data of temperature-dependent thermal conductivities for amorphous GST, the temperature-dependent thermal conductivities of amorphous $GeTe_4$ are predicted and compared with the results from previous steady-state measurements [25]. Prediction results based on the MTC model and AF theory with constant broadening are also presented in figure 4(a), shown as purple dashed line and solid red line, respectively. For the MTC model, the calculation formula [39] is

$$\kappa^{\mathrm{MTC}} = \left(\frac{\pi}{6}\right)^{1/3} k_{\mathrm{B}} n^{2/3} \sum_i v_i \left(\frac{T}{\theta_i}\right)^2 \int_0^{\theta_i/T} \frac{x^3 e^x}{\left(e^x-1\right)^2} \mathrm{d}x, \quad (16)$$

in which n is the density of atoms per unit volume (3.01×10^{23} m^{-3} for amorphous $GeTe_4$ [25]), and the summation is operated over three polarizations (i represents longitudinal or transverse modes). The cut-off of each integral is determined by

$$\theta_i = v_i \left(h/k_{\mathrm{B}}\right) \left(6\pi^2 n\right)^{1/3}, \quad (17)$$

v_i is approximated by measured sound velocity (1.19 km s^{-1} for amorphous $GeTe_4$ [25]) for longitudinal mode, and the

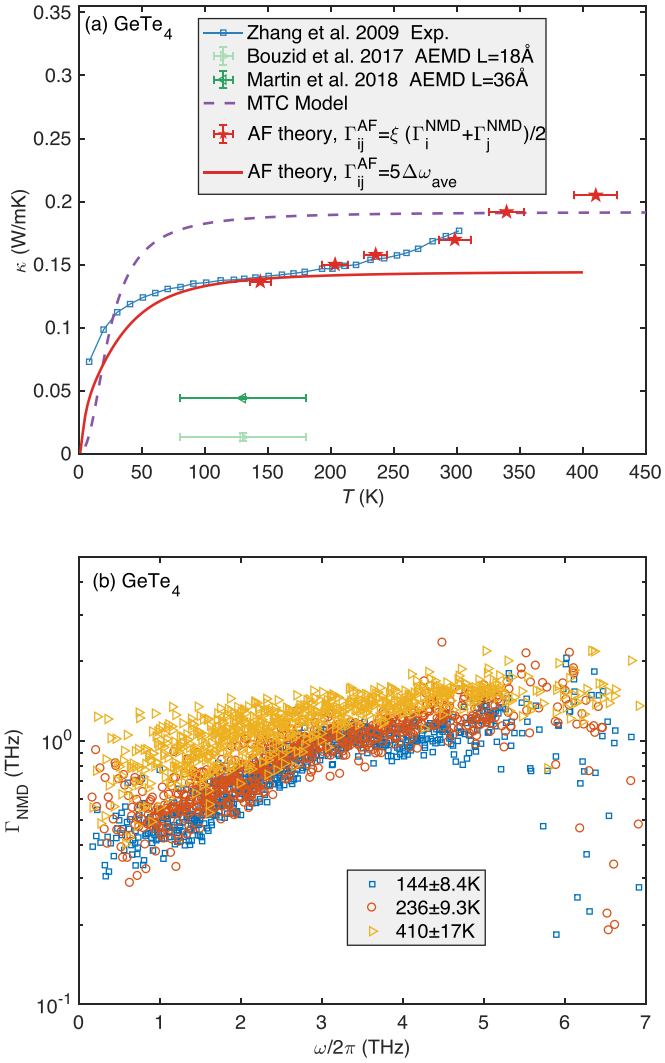

Figure 4. (a) Thermal conductivities of amorphous $GeTe_4$ at various temperatures from experiments [25], AEMD [34–36], and predicted by AF theory with NMD linewidths dependent broadening, and temperature dependence predicted by MTC model [39] and broadening with constant broadening. Prediction results from AEMD are given, with the error bars of AEMD results are from the existing temperature difference while the error bars of AF theory-predicted results are from temperature fluctuation in the NVE ensemble. (b) Linewidths of amorphous $GeTe_4$ predicted by NMD at various temperatures.

relationship between the longitudinal sound velocity v_l and transverse v_t ($v_l = 1.65v_t$) is also used, according to [25, 77]. As for the AF theory with the constant broadening method, $5\Delta\omega_{ave}$ is used as the broadening width. Both the MTC model and AF theory with constant broadening agree well with the experimental results below Debye temperature but predict temperature-independent thermal conductivities in higher temperatures, notably different with the positive temperature dependence from the experiments [25]. The thermal conductivities at various temperatures are also predicted by AF theory with the NMD mode linewidths dependent broadening method, shown as red pentagrams in figure 4(a), which agree well with experimental results, qualitatively. The temperature error bars are from the standard deviation of temperature fluctuation during the simulations in NVE at corresponding temperatures, which are much smaller than the existing temperature differences in AEMD simulations (see green error bars of the triangles in figure 4(a)). We note that the calculation frameworks used in this paper are in equilibrium so as to allow predictions and reliable analyses on temperature-dependent thermal conductivities. Here, only coherences' contribution is considered because the populations' contribution for each case is below 2.5%, neglectable for the amorphous $GeTe_4$ sample. For predictions on coherences' contribution, ξ is chosen as 0.033 and remains consistent for cases at various temperatures. We claim that the consideration of anharmonicity by the linewidths dependent broadening method results in the good agreement of temperature dependence between the predictions in this paper and the experimental results, and it is coherences' contribution that dominates the characteristics of heat conduction in amorphous $GeTe_4$. The larger mode linewidths at higher temperatures, shown in figure 4(b), result in the stronger coupling between vibrational modes, leading to the larger coherences' contribution, described by equations (9), (13), and (14). This is quite different from the phonon-like populations' contribution, which will be smaller due to the suppressed lifetimes, corresponding to the larger linewidths, at higher temperatures.

4. Conclusions

In summary, we combined the AF theory and SMA to investigate the vibrational thermal conductivity of amorphous PCMs based on a first-principles calculation. A mode linewidths-dependent broadening method is introduced, inspired by the anharmonic term in the exact formula of the coherences' contribution. The new broadening method is adopted in the AF theory to predict the coherences' contribution, and the SMA based on NMD is used to predict the populations' contribution. The predicted value of the thermal conductivity of amorphous GST at 300 K is 0.25 ± 0.04 W m^{-1} K^{-1}, and the coherences' contribution (98.5%) dominates the heat conduction while the populations' contribution (1.5%) could be neglected. The temperature-dependent thermal conductivities of amorphous $GeTe_4$ are also predicted by the same framework and turn out to be in good agreement with the experimental results above the Debye temperature, which are beyond the MTC model or AF theory with the constant broadening. Our calculation offers new insight into thermal transport in amorphous PCM materials and reveals the underlying physical mechanisms of the positively temperature-dependent thermal conductivities above Debye temperature.

Data availability statement

The data generated and/or analyzed during the current study are not publicly available for legal/ethical reasons but are available from the corresponding author on reasonable request.

Acknowledgments

The authors thank Dr. Y. C. Hua at the Department of Mechanical Engineering at the University of Tokyo for helpful discussions. This work was supported by the National Natural Science Foundation of China (Nos. 51825601 and U20A20301).

ORCID iD

Bing-Yang Cao https://orcid.org/0000-0003-3588-972X

References

[1] Zhang W, Mazzarello R, Wuttig M and Ma E 2019 *Nat. Rev. Mater.* **4** 150
[2] Wong H-S P, Raoux S, Kim S, Liang J, Reifenberg J P, Rajendran B, Asheghi M and Goodson K E 2010 *Proc. IEEE* **98** 2201
[3] Abdollahramezani S, Hemmatyar O, Taghinejad H, Krasnok A, Kiarashinejad Y, Zandehshahvar M, Alù A and Adibi A 2020 Tunable Nanophotonics Enabled by Chalcogenide Phase-Change Materials *Nanophotonics* **9** 1189–241
[4] Zhang W, Mazzarello R and Ma E 2019 *MRS Bull.* **44** 686
[5] Wu L C *et al* 2016 *Sci. Sin. Phys. Mech. Astron.* **46** 107309
[6] Bozorg-Grayeli E, Reifenberg J P, Asheghi M, Wong H-S P and Goodson K E 2013 *Annu. Rev. Heat Transfer* **16** 397
[7] Sosso G C, Deringer V L, Elliott S R and Csányi G 2018 *Mol. Simul.* **44** 866
[8] Song W-X, Cheng Y, Cai D, Tang Q, Song Z, Wang L, Zhao J, Xin T and Liu Z-P 2020 *J. Appl. Phys.* **128** 075101
[9] Mocanu F C, Konstantinou K and Elliott S R 2020 *Appl. Phys. Lett.* **116** 031902
[10] Sosso G C, Donadio D, Caravati S, Behler J and Bernasconi M 2012 *Phys. Rev.* B **86** 104301
[11] Lyeo H K, Cahill D G, Lee B S, Abelson J R, Kwon M H, Kim K B, Bishop S G and Cheong B K 2006 *Appl. Phys. Lett.* **89** 87
[12] Kuwahara M, Suzuki O, Yamakawa Y, Taketoshi N, Yagi T, Fons P, Fukaya T, Tominaga J and Baba T 2007 *Japan. J. Appl. Phys.* **46** 3909
[13] Reifenberg J P, Panzer M A, Kim S, Gibby A M, Zhang Y, Wong S, Wong H S P, Pop E and Goodson K E 2007 *Appl. Phys. Lett.* **91** 1
[14] Lee J, Bozorg-Grayeli E, Kim S, Asheghi M, Philip Wong H-S and Goodson K E 2013 *Appl. Phys. Lett.* **102** 191911
[15] Levin E M, Besser M F and Hanus R 2013 *J. Appl. Phys.* **114** 83713
[16] Warzoha R J, Donovan B F, Vu N T, Champlain J G, Mack S and Ruppalt L B 2019 *Appl. Phys. Lett.* **115** 023104
[17] Ghosh K, Kusiak A, Noé P, Cyrille M C and Battaglia J L 2020 *Phys. Rev.* B **101** 214305
[18] Giraud V, Cluzel J, Sousa V, Jacquot A, Dauscher A, Lenoir B, Scherrer H and Romer S 2005 *J. Appl. Phys.* **98** 013520
[19] Risk W P, Rettner C T and Raoux S 2008 *Rev. Sci. Instrum.* **79** 26108
[20] Risk W P, Rettner C T and Raoux S 2009 *Appl. Phys. Lett.* **94** 101906
[21] Lan R, Endo R, Kuwahara M, Kobayashi Y and Susa M 2012 *J. Appl. Phys.* **112** 053712
[22] Fallica R, Varesi E, Fumagalli L, Spadoni S, Longo M and Wiemer C 2013 *Phys. Status Solidi* **7** 1107
[23] Siegert K S, Lange F R L, Sittner E R, Volker H, Schlockermann C, Siegrist T and Wuttig M 2014 *Rep. Prog. Phys.* **78** 13001
[24] Huang Y-H and Hsieh T-E 2015 *Int. J. Therm. Sci.* **87** 207
[25] Zhang S N, He J, Zhu T J, Zhao X B and Tritt T M 2009 *J. Non. Cryst. Solids* **355** 79
[26] Reifenberg J 2010 Thermal Phenomena in Phase Change Memory *PhD* Stanford University
[27] Bao H, Chen J, Gu X and Cao B 2018 A Review of Simulation Methods in Micro/Nanoscale Heat Conduction *ES Energy Environ.* **1** 16-55
[28] Fugallo G, Lazzeri M, Paulatto L and Mauri F 2013 *Phys. Rev.* B **88** 045430
[29] Li W, Carrete J, Katcho N A and Mingo N 2014 *Comput. Phys. Commun.* **185** 1747
[30] Campi D, Paulatto L, Fugallo G, Mauri F and Bernasconi M 2017 *Phys. Rev.* B **95** 024311
[31] Ibarra-Hernández W and Raty J Y 2018 *Phys. Rev.* B **97** 1
[32] Pan Y, Li Z and Guo Z 2019 *Crystals* **9** 136
[33] Duong T-Q, Bouzid A, Massobrio C, Ori G, Boero M and Martin E 2021 *RSC Adv.* **11** 10747
[34] Bouzid A, Zaoui H, Luca Palla P, Ori G, Boero M, Massobrio C, Cleri F and Lampin E 2017 *Phys. Chem. Chem. Phys.* **19** 9729
[35] Martin E, Palla P L, Cleri F, Bouzid A, Ori G, Le Roux S, Boero M and Massobrio C 2018 *J. Non. Cryst. Solids* **498** 190
[36] Duong T Q, Massobrio C, Ori G, Boero M and Martin E 2019 Thermal conductivity and transport modes in glassy GeTe 4 by first-principles molecular dynamics *Phys. Rev. Mater.* **3** 105401
[37] Einstein A 1911 *Ann. Phys.* **340** 679
[38] Slack G A 1979 The Thermal Conductivity of Nonmetallic Crystals *Solid State Phys.* **34** 1–71
[39] Cahill D G, Watson S K and Pohl R O 1992 *Phys. Rev.* B **46** 6131
[40] Wingert M C, Zheng J, Kwon S and Chen R 2016 *Semicond. Sci. Technol.* **31** 113003
[41] Winter M R and Clarke D R 2006 *Acta Mater.* **54** 5051
[42] Fang J, Reitz C, Brezesinski T, Nemanick E J, Kang C B, Tolbert S H, Tolbert S H and Pilon L 2011 *The Journal of Physical Chemistry C* 115 p 14606–14
[43] Cappella A, Battaglia J, Schick V, Kusiak A, Lamperti A, Wiemer C and Hay B 2013 *Adv. Eng. Mater.* **15** 1046
[44] Lv W and Henry A 2016 *Sci. Rep.* **6** 4
[45] Gurlo A, Ionescu E, Riedel R and Clarke D R 2016 *J. Am. Ceram. Soc.* **99** 281
[46] Allen P B and Feldman J L 1993 *Phys. Rev.* B **48** 12581
[47] Hardy R J 1963 *Phys. Rev.* **132** 168
[48] Simoncelli M, Marzari N and Mauri F 2019 *Nat. Phys.* **15** 809
[49] Allen P B, Feldman J L, Fabian J and Wooten F 1999 *Phil. Mag.*B **79** 1715
[50] Feldman J L, Kluge M D, Allen P B and Wooten F 1993 *Phys. Rev.* B **48** 12589
[51] Larkin J M and McGaughey A J H 2014 *Phys. Rev.* B **89** 144303
[52] Zhou Y, Morshedifard A, Lee J and Abdolhosseini Qomi M J 2017 *Appl. Phys. Lett.* **110** 043104
[53] Tambo N, Liao Y, Zhou C, Ashley E M, Takahashi K, Nealey P F, Naito Y and Shiomi J 2020 *Sci. Adv.* **6** eabc0075
[54] Luo Y, Yang X, Feng T, Wang J and Ruan X 2020 *Nat. Commun.* **11** 2554
[55] Sosso G C, Miceli G, Caravati S, Behler J and Bernasconi M 2012 Neural network interatomic potential for the phase change material GeTe *Phys. Rev.* B **85** 174103
[56] DeAngelis F, Muraleedharan M G, Moon J, Seyf H R, Minnich A J, McGaughey A J H and Henry A 2019 *Nanoscale Microscale Thermophys. Eng.* **23** 81

[57] Zhou W X, Cheng Y, Chen K Q, Xie G, Wang T and Zhang G 2020 *Adv. Funct. Mater.* **30** 1903829
[58] Allen P B and Feldman J L 1989 *Phys. Rev. Lett.* **62** 645
[59] Mcgaughey A J H and Larkin J M 2014 *Annu. Rev. Heat Transfer* **17** 49
[60] Tang D S, Qin G Z, Hu M and Cao B Y 2020 *J. Appl. Phys.* **127** 1
[61] Tang D S and Cao B Y 2021 *J. Appl. Phys.* **129** 085102
[62] Kresse G and Furthmüller J 1996 *Phys. Rev.* B **54** 11169
[63] Kresse G and Joubert D 1999 *Phys. Rev.* B **59** 1758
[64] Perdew J P, Burke K and Ernzerhof M 1996 *Phys. Rev. Lett.* **77** 3865
[65] Togo A and Tanaka I 2015 *Scr. Mater.* **108** 1
[66] Stachurski Z H 2015 *Fundamentals of Amorphous Solids: Structure and Properties* (New York: Wiley)
[67] Mocanu F C, Konstantinou K, Lee T H, Bernstein N, Deringer V L, Csányi G and Elliott S R 2018 *J. Phys. Chem.* B **122** 8998
[68] Grimme S 2006 *J. Comput. Chem.* **27** 1787
[69] Jóvári P, Kaban I, Steiner J, Beuneu B, Schöps A and Webb M A 2008 *Phys. Rev.* B **77** 35202
[70] Njoroge W K, Wöltgens H-W and Wuttig M 2002 *J. Vac. Sci. Technol.* A **20** 230
[71] Kaban I, Halm T, Hoyer W, Jovari P and Neuefeind J 2003 *J. Non. Cryst. Solids* **326** 120
[72] Silvestrelli P L, Martin E, Boero M, Bouzid A, Ori G and Massobrio C 2020 *J. Phys. Chem.* B **124** 11273–9
[73] Mocanu F C, Konstantinou K and Elliott S R 2020 *J. Phys. D: Appl. Phys.* **53** 244002
[74] Konstantinou K, Mavračić J, Mocanu F C and Elliott S R 2020 *Phys. Status Solidi* 2000416
[75] Gibbons J D and Chakraborti S 2014 *Nonparametric Statistical Inference: Revised and Expanded* (Boca Raton, FL: CRC Press)
[76] Das Gupta S 1960 Point biserial correlation coefficient and its generalization *Psychometrika* **25** 393
[77] Berret J F and Meissner M 1988 *Z. Phys.* B **70** 65